Available online at www.sciencedirect.com
ScienceDirect
Trans. Nonferrous Met. Soc. China 31(2021) 3613−3625
Transactions of Nonferrous Metals Society of China
www.tnmsc.cn

Comparison of wear behaviour of LM13 Al−Si alloy based composites reinforced with synthetic (B_4C) and natural (ilmenite) ceramic particles

Rahul GUPTA[1], Tarun NANDA[1], O. P. PANDEY[2]

1. Mechanical Engineering Department, Thapar Institute of Engineering and Technology, Patiala 147004, Punjab, India;
2. School of Physics and Materials Science, Thapar Institute of Engineering and Technology, Patiala 147004, Punjab, India

Received 20 December 2020; accepted 28 June 2021

Abstract: Dry sliding wear behaviour of stir-cast aluminium matrix composites (AMCs) containing LM13 alloy as matrix and ceramic particles as reinforcement was investigated. Two different ceramic particle reinforcements were used separately: synthetic ceramic particles (B_4C), and natural ceramic particles (ilmenite). Optical micrographs showed uniform dispersion of reinforced particles in the matrix material. Reinforced particles refined the grain size of eutectic silicon and changed its morphology to globular type. B_4C reinforced composites (BRCs) showed maximum improvement in hardness of AMCs. Ilmenite reinforced composites (IRCs) showed maximum reduction in coefficient of friction values due to strong matrix−reinforcement interfacial bonding caused by the formation of interfacial compounds. Dry sliding wear behaviour of composites was significantly improved as compared to base alloy. The low density and high hardness of B_4C particles resulted in high dislocation density around filler particles in BRCs. On the other hand, the low thermal conductivity of ilmenite particles resulted in early oxidation and formation of a tribo-layer on surface of IRCs. So, both types of reinforcements led to the improvement in wear properties of AMCs, though the mechanisms involved were very different. Thus, the low-cost ilmenite particles can be used as alternative fillers to the high-cost B_4C particles for processing of wear resistant composites.

Key words: aluminium matrix composites; ilmenite; boron carbide; particle-reinforcement; wear test; tribolayer; XRD analysis; SEM−EDS

1 Introduction

Dry sliding wear characteristics are important in applications such as bearings, cams, gears, and brake rotors, as the metal−metal contact in these applications causes wear of surfaces [1,2]. Wear of materials results in a decrease in working efficiency and life cycle [3]. The materials currently being used in such applications are of high density which increases the overall weight of vehicle and results in decreased fuel efficiency [2,4]. To increase the working efficiency and also life cycle, researchers have been studying the dry sliding wear characteristics of aluminium matrix composites (AMCs) by adding ceramic particles as reinforcement [5−7]. The results obtained are encouraging which show that AMCs can be used in different sectors viz. automobile, aerospace, and defence [8−10]. Ceramic particles are used as reinforcement due to their high hardness, high stability, low thermal-conductivity, low thermal-expansion coefficient, and high strength and modulus [4,11−13].

Two types of ceramic particles are used by researchers viz. (1) synthetic ceramic particles, and (2) natural ceramic particles. Synthetic ceramic particles listed in literature include SiC, TiC, TiB_2,

Corresponding author: O. P. PANDEY, Tel: +91-98884-01777, +91-175-2393893, E-mail: oppandey@gmail.com, oppandey@thapar.edu
DOI: 10.1016/S1003-6326(21)65752-7

B_4C, WC, Al_2O_3, etc [13−18]. However, zircon, sillimanite, rutile, garnet, etc, are some commonly-used natural ceramic particles [2,12,13,19]. Synthetic ceramics have high hardness, good chemical and thermal stability [1,4]. However, they have poor wettability with matrix material. Hence, the bond formed between matrix and reinforcement is weak, which decreases the load bearing capacity of the composites [20,21]. Also, synthetic ceramics are available at a high cost [13]. On the other hand, natural ceramics possess almost similar favourable properties (high values of hardness, thermal stability, melting point, and strength) as those possessed by synthetic ceramics. However, these natural minerals provide additional benefits viz. lower coefficient of friction, lower thermal conductivity, and lesser difference in coefficient of thermal expansion of matrix and reinforced natural minerals [2,12,22]. Further, natural ceramics occur in abundance in the coastal areas and hence are available at low-cost. The use of these non-expensive natural ceramics results in the development of economical AMCs [2,23].

ZENG et al [24] studied the wear characteristics of a hypoeutectic Al−Si alloy by adding reduced graphene oxide (RGO) and silicon carbide particles. Increase in stability of friction film by RGO particles and increase in hardness of composites by SiC particles resulted in improved wear behaviour of the processed composites. GUPTA et al [13] studied the effect of reinforcing rutile and sillimanite particles on the wear behaviour of LM27 aluminium alloy. Rutile particles refined the microstructure and also provided increased lubricity effect. Sillimanite particles resulted in high hardness and formation of strong matrix−reinforcement interfacial bonding. Literature revealed that synthetic ceramic fillers (SiC, B_4C etc) significantly improve the wear characteristics of composites; however, their high cost increases the overall cost of processing the composites [2,13,24]. To overcome this problem of high cost of processing, the present research was taken up to compare the wear behaviour of AMCs reinforced with a high-cost synthetic ceramic filler (boron carbide particles) and those reinforced with a low-cost naturally occurring mineral (ilmenite particles). The main objective/novelty was to determine if the natural occurring ceramic fillers could substitute the high-cost synthetic ceramic fillers. In the present work, boron carbide was used as the synthetic ceramic particle reinforcement because of its low density, low coefficient of thermal expansion, high hardness, high strength, high melting point, and high impact strength [1,20]. On the other hand, ilmenite was used as the natural ceramic particle reinforcement. Ilmenite possesses high melting point, high thermal stability, low thermal conductivity, and low coefficient of thermal expansion [25]. Ilmenite is an economical industrial ore of titanium available at various locations of the Indian subcontinent including the states of Kerala, Tamil Nadu, Odisha, and Andhra Pradesh [26].

2 Experimental

2.1 Starting materials and processing of AMCs

LM13 alloy (composition shown in Table 1) was used as the matrix material. It is a frequently used Al−Si alloy for making engine components. LM13 alloy possesses good fluidity, high strength and low coefficient of thermal expansion. These properties are sustainable at elevated temperatures also [27−29].

Table 1 Elemental composition of LM13 base alloy (wt.%)

Si	Mg	Cu	Fe	Mn	Ni
12.00	0.11	1.10	0.80	0.40	1.20
Zn	Pb	Sn	Ti	Al	
0.05	0.07	0.07	0.18	Bal.	

AMCs processed in the present research contained a single reinforcement, either (1) boron carbide particles (synthetic ceramic), or (2) ilmenite particles (natural ceramic). The SEM−EDS analysis results of reinforced particles are presented in Fig. 1. Particle size range of both reinforcements was same and in the range of 106−125 μm. Table 2 presents the designations used for various fabricated AMCs.

The base alloy (LM13) was melted in the stir casting set-up using an electric furnace maintained at 973 K. Ceramic particles (reinforcement) were pre-heated in another electric furnace maintained at 723 K to eliminate moisture/volatile matter from the particles. Before addition of pre-heated particles, a vortex was developed in the molten mass by using a three-blade graphite stirrer. Uniform stirring at 650 r/min was maintained for 10 min. Thereafter,

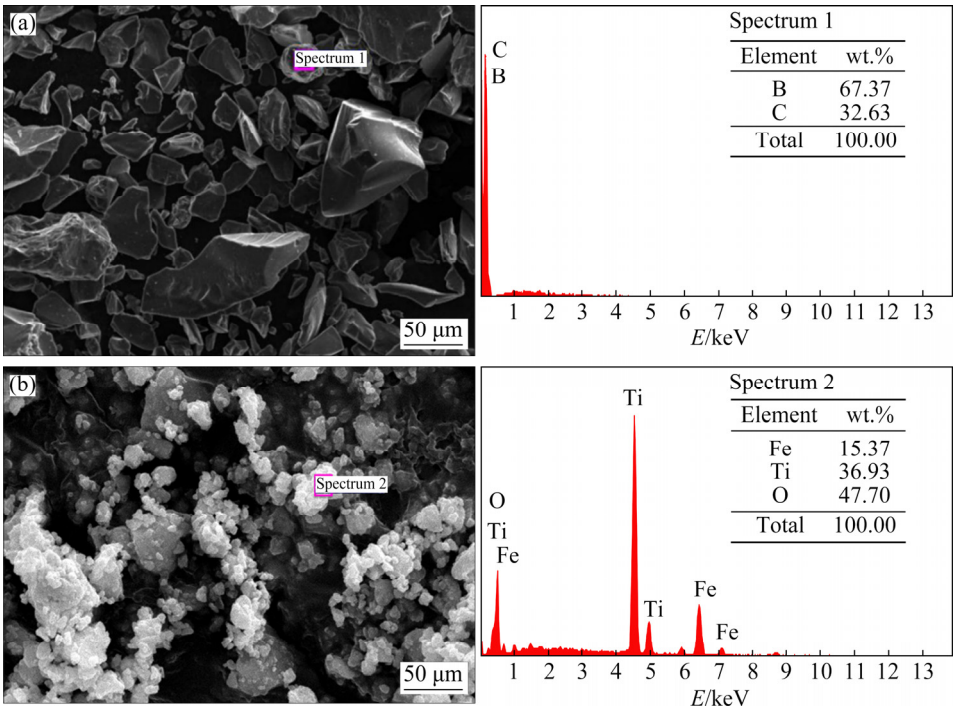

Fig. 1 SEM−EDS analysis results of boron carbide particles (a) and ilmenite particles (b)

Table 2 Designation used for AMCs

Reinforcement level/wt.%	Designation	
	Boron carbide reinforced composites (BRC)	Ilmenite reinforced composites (IRC)
5.0	BRC-5	IRC-5
10.0	BRC-10	IRC-10
15.0	BRC-15	IRC-15

the required amount of particles were added in the molten mass by reducing the stirring speed to 250 r/min. Again, stirrer was maintained at 650 r/min for 10 min. Finally, pouring of molten mass was done in a cast iron mould to allow cooling till room temperature.

2.2 Testing of AMCs

Billets obtained after stir casting were machined to obtain cylindrical pins with diameter of 8 mm and length of 90 mm for wear testing (G99−05 ASTM standard). Wear tests were performed on pin-on-disc set-up, where test-pin slides against EN31 steel disc (sliding-speed: 1.6 m/s; sliding-distance: 3000 m). Pins were subjected to different loads viz. 9.8, 29.4, and 49.0 N.

During wear testing, the height lost by cylindrical pins was measured using a LVDT with accuracy of 1 μm. This height loss was used to obtain the wear rate (R_W) as

$$R_W = \frac{H \cdot C}{S} \quad (1)$$

where H is the height loss, C is the contact area of cylindrical pin with steel disc, and S is teh sliding distance with respect to height loss.

Surface roughness tester (SJ400, Mitutoyo; least count: 0.001 μm) was used to determine the surface roughness of (1) composite samples before the wear/friction tests, and (2) steel disc of the wear testing machine. The roughtness (R_a) values obtained for the composite samples and the steel disc were in the range of (31±5) and (24±3) μm, respectively. Also, hardness (HRB value) of the processed AMCs was determined using a Rockwell hardness tester (indenter: tempered steel ball; major load: 980 N; dwell time: 10 s). For each sample, five indentations were obtained to calculate the mean hardness value. Similarly, wear test for a given condition was performed thrice to obtain the average wear rate value.

2.3 Characterisation of AMCs

Standard metallurgical procedure was used to obtain a mirror finish on flat surfaces of cylindrical pins for microstructural analysis. After mirror

finishing, surfaces were analysed under optical microscope to note the changes occurring at micro-level after the addition of reinforced particles to the base alloy. Formation of new phases and presence of reinforced particles in AMCs were confirmed using X-ray diffractograms. Further, SEM−EDS analysis of wear tracks and wear debris was conducted to determine the wear-mechanisms causing materials loss.

3 Results and discussion

3.1 Characterization results

XRD patterns of AMCs containing maximum reinforcement level i.e. BRC-15 and IRC-15 composites are presented in Fig. 2.

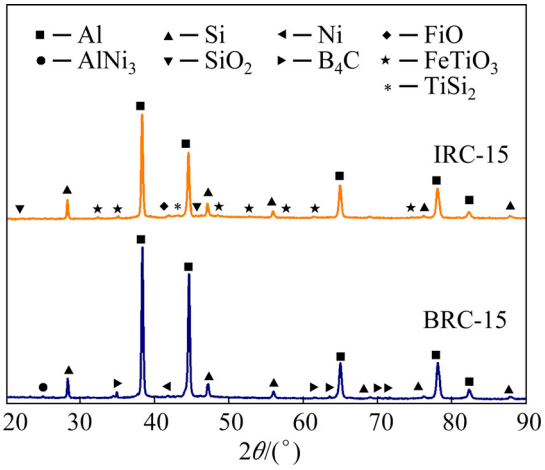

Fig. 2 XRD patterns of IRC-15 and BRC-15 composites

XRD patterns of both the composites showed peaks of aluminium (Al) and silicon (Si) which correspond to LM13 base alloy. Further, several other peaks were observed which indicated the presence of reinforced particles, formation of intermetallic compounds, and/or occurrence of interfacial reaction products. BRC-15 composites showed additional peaks indicating the presence of boron carbide (B_4C), nickel (Ni), and aluminium−nickel ($AlNi_3$) phases. IRC-15 composites showed additional peaks indicating the presence of ilmenite ($FeTiO_3$), silicon oxide (SiO_2), iron oxide (FeO), and titanium−silicon ($TiSi_2$) phases. Aluminium−nickel phase in BRC composites showed formation of intermetallic compounds (this phase was absent in IRC-15 composites). Further, an additional metallic phase (Ni) was also observed in BRC composites. In the case of IRC composites, the presence of silicon oxide, iron oxide, and titanium−silicon phases signified the formation of interfacial products through reaction between reinforced particles (ilmenite) and the matrix material (silicon of the base alloy). The interfacial reaction can be described as

$$3Si+FeTiO_3 \rightarrow FeO+SiO_2+TiSi_2 \quad (2)$$

No such interfacial reaction was observed for B_4C composites. It is reported that occurrence of interfacial reaction on reinforced particles results in better wetting behaviour [20,30,31]. So, formation of interfacial products on $FeTiO_3$ (ilmenite particles) may result in formation of relatively stronger interfacial bonding in IRC composites.

Table 3 presents the average crystallite size and crystallinity (obtained from X-ray diffractograms) for the base alloy and various composites. Addition of reinforced particles to the base alloy reduced the crystallite size and increased the crystallinity of composites. Further, relatively lower crystallite size and higher crystallinity were observed for boron carbide reinforced composites.

Table 3 Crystallite size and crystallinity of base alloy, IRC-15 and BRC-15 composites

Type of AMC	Average crystallite size/nm	Crystallinity/ %
LM13 alloy	65.74	30
IRC-15	45.56	55
BRC-15	41.60	63

Rise in crystallinity of composites signifies an increase in nucleation rate of new crystals. This increase in nucleation rate causes the formation of crystallites of smaller size, i.e. decrease in average crystallite size. Further, the crystallite size shows an inverse relationship with dislocation density [32−34]. Thus, the rise in crystallinity and decrease in crystallite size signify the presence of higher dislocation density in BRC-15 composite, and hence, higher hardness as compared to IRC-15 composite.

Optical micrograph of LM13 alloy shows the presence of two main regions, i.e. (1) primary Al, and (2) eutectic mixture of Al−Si (Fig. 3(a)). During casting, initially primary α(Al) nucleates in the molten mass and as the temperature decreases, it grows as dendrites. When temperature reaches 850 K, the eutectic mixture nucleates in the molten

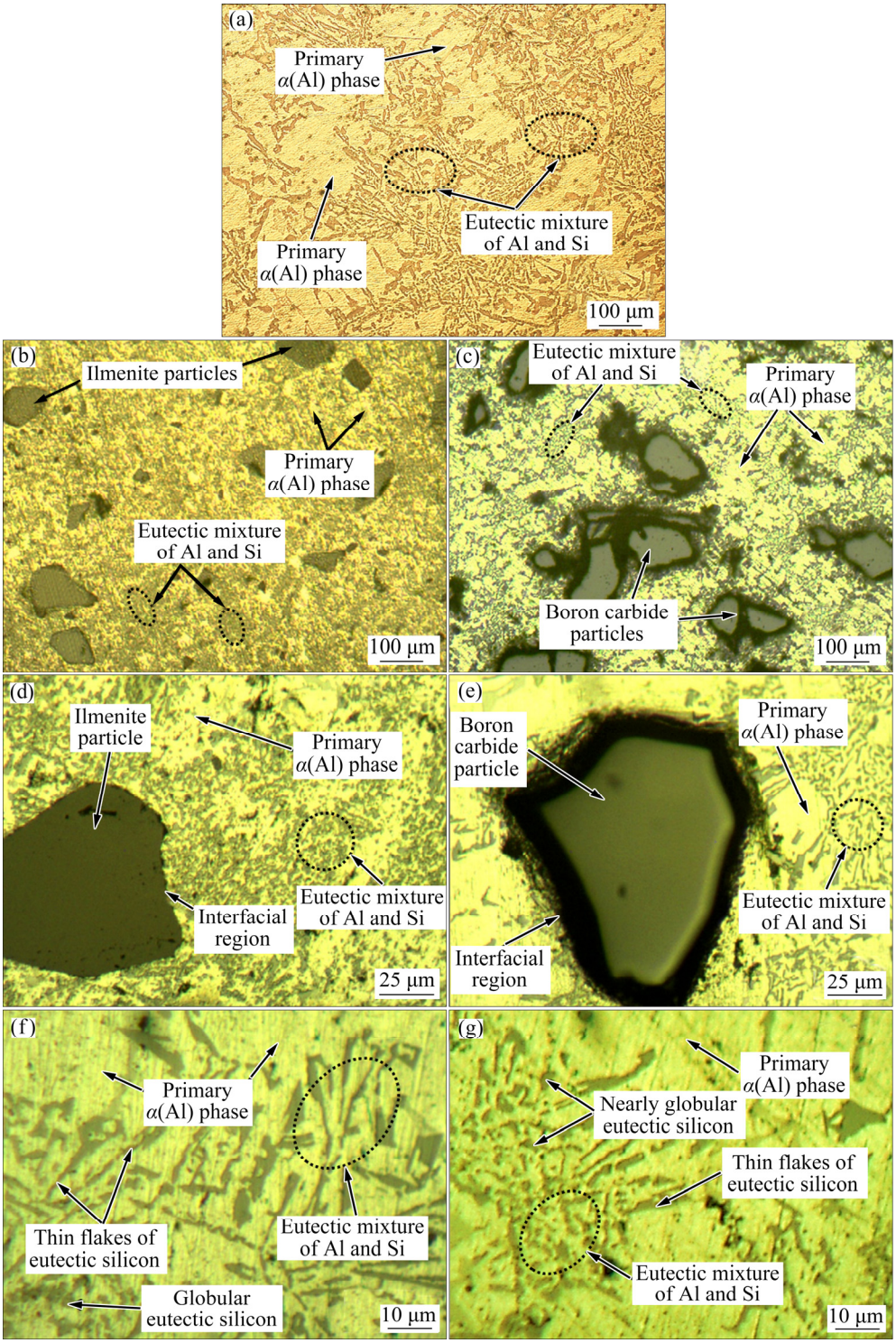

Fig. 3 Micrographs of as-cast LM13 alloy (a), IRC-15 (b−d), and BRC-15 (e−g)

mass around the dendrites of α(Al). In the present research, cooling rate was quite low. Low cooling rate decreases the number of nuclei and allows the formed nuclei to grow. This growth of nuclei results in the formation of larger grains [3,28]. Further, Si phase present in the as-cast LM13 alloy was flaky-shaped.

Figures 3(b, d, f) and Figs. 3(c, e, g) present the optical micrographs of IRC-15 and BRC-15 composites, respectively. The micrographs revealed that for both types of composites, the reinforced particles were uniformly distributed in the matrix. Ceramic particles were observed to be present in the vicinity of eutectic silicon. The flake-like eutectic

silicon morphology in base alloy was changed to nearly globular in AMCs. Globular morphology of eutectic silicon was mostly observed in BRC composites, which signified that B_4C particles were more effective in refinement of silicon phase as compared to $FeTiO_3$ particles.

For composites, the solidification process depends on thermal conductivity of reinforced particles. If thermal conductivity of reinforced particles is high, the cooling rate of molten mass around the reinforced particles is also high. Thermal conductivity values of base alloy, B_4C particles, and $FeTiO_3$ particles are 166, 30 and 1.49 W/(m·K), respectively [11,35]. During the solidification process, the reinforced particles were not able to cool at a rate as fast as that of base alloy due to their low thermal conductivity. These ceramic particles acted as a heat source, not allowing the molten mass in their surroundings to cool down. As a result, nucleation of primary α(Al) occurred away from the reinforced particles, as shown in Fig. 3 [2]. During the growth of these nuclei, some of the reinforced ceramic particles were pushed and got entrapped in the inter-dendritic regions. After solidification of primary α(Al), most of the regions around ceramic particles were still in the molten state. Hence, ceramic particles were considered as primary sites for solidification of eutectic phase. Cooling rate around B_4C particles was higher as compared to $FeTiO_3$ particles because of the higher thermal conductivity of B_4C. This higher cooling rate was responsible for the increased number of nuclei, and hence finer grains in B_4C composites (Figs. 3(f, g)) [3,28].

3.2 Hardness results

Figure 4 shows the hardness values of various BRC and IRC composites. There was increase in hardness of AMCs with the increase in reinforcement level. Further, BRC composites showed relatively higher hardness. The increase in hardness with the addition of reinforced particles was attributed to the increase in resistance to plastic deformation [15].

Hardness of AMCs is also influenced by (1) mismatch in coefficient of thermal expansion (CTE) values of reinforcement and matrix, and (2) grain size of base alloy [12,13]. The CTE values for LM13 alloy, B_4C particles, and $FeTiO_3$ particles are 20.29×10^{-6}, 3.20×10^{-6} and $27.90\times10^{-6}\,K^{-1}$, respectively [4,8,36]. Higher mismatch in CTE values of matrix and reinforcement increases the dislocation density in AMCs, thereby resulting in higher hardness [13]. For this reason, (1) hardness of AMCs increased with the increase in reinforcement level, and (2) BRC composites showed higher hardness at a given reinforcement level. Hardness of AMCs also increases with the decrease in grain size. For this reason also, BRC composites which resulted in more refinement of eutectic silicon showed higher hardness. XRD analysis of BRC-15 composite showed higher crystallinity and lower crystallite size, which also confirmed its relatively higher hardness (compared to IRC composites).

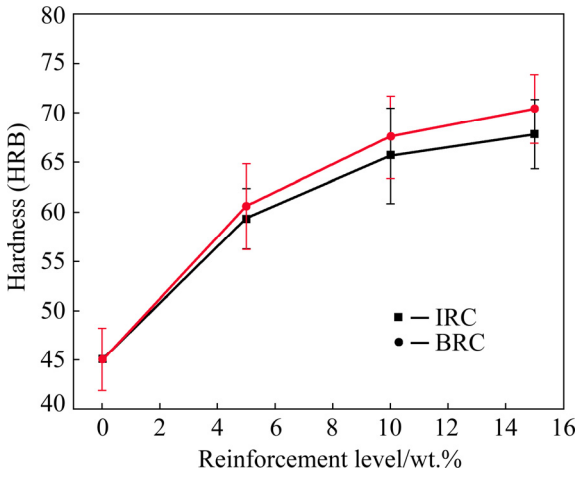

Fig. 4 Hardness of base alloy, BRC composites and IRC composites at various reinforcement levels

3.3 Tribological behaviour

Figure 5 presents the wear rate of various formulations as a function of sliding distance under various applied loads.

3.3.1 Influence of sliding distance

The wear graphs (of base alloy and AMCs) showed three distinct wear regions based on the sliding distance: (1) region showing sharp increase in wear rate for sliding distance in the range of 0−500 m, (2) region showing sharp decrease in wear rate for sliding distance in the range 500−2000 m, and (3) region showing no significant change in wear rate for sliding distance in the range of 2000−3000 m. During the initial stage of sliding, asperities of pin and disc surface make contact with each other as both have different surface roughness [13]. For pin, the roughness value (R_a) was (31±5) μm, and for disc, it was (24±3) μm.

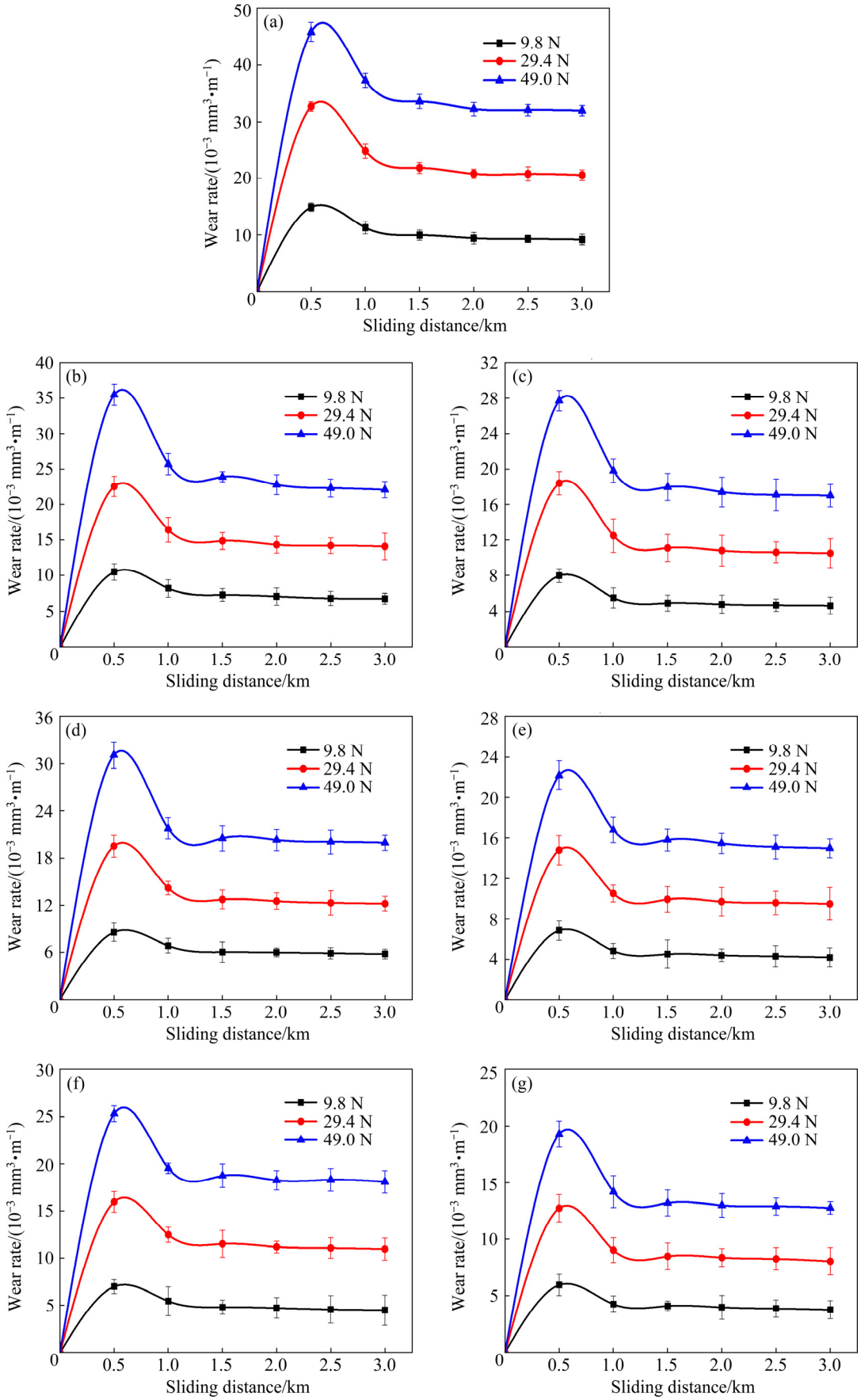

Fig. 5 Wear rate as function of sliding distance under various loads for LM13 alloy (a), and various AMCs (b−g): (b) IRC-5; (c) BRC-5; (d) IRC-10; (e) BRC-10; (f) IRC-15; (g) BRC-15

Under the action of applied load, these asperities deformed plastically and got fractured, which led to rise in wear rate for sliding distance of 0−500 m. This resulted in the formation of wear debris which either got trapped between the sliding surfaces or moved out of the system [5,13]. Also, the stress acting due to applied load on both, the sliding surface (i.e. worn surface of pin) and the entrapped debris led to strain hardening [6,37]. Strain hardening of pin was mainly responsible for the decrease in wear rate in the sliding range of 500−2000 m. The entrapment of wear debris and the phenomenon of strain hardening lead to the formation of a hard mechanical mixed layer (MML) between pin and disc surface [5]. MML or tribolayer comprises matrix material, counter surface material, reinforced particles, and their respective oxides. The presence of oxides was attributed to friction acting between both the surfaces [6,7].

CHEN and ALPAS [37] provided relationship for the maximum temperature (T_{max}) obtained on the worn surface:

$$T_{max}=T_0+a\cdot F^{1/4}\cdot v^{1/2} \quad (3)$$

where F is applied load, v is sliding velocity, and T_0 and a are constants. The values of T_0 and a depend on values of F and v. If $(F^{1/4}\cdot v^{1/2})$ is less than 2.8, T_0 and a are equal to 290 K and 15.1, respectively. Otherwise, the values are −191 K and 210.5, respectively. For sliding speed of 1.6 m/s, the maximum temperature attained under various applied loads is given in Table 4.

This temperature rise on the worn surface contributes towards the formation of an oxide film on the surface of pin. Attainment of steady state wear was attributed to the oxidation of sliding surfaces and the formation of mechanically mixed layer (MML) [5].

Table 4 Maximum temperature predicted on pin surface under different applied loads

Sliding velocity/ ($m\cdot s^{-1}$)	Applied load/N	T_0/K	a	Maximum temperature at sliding surface/K
1.6	9.8	290	15.1	324
1.6	29.4	−191	210.5	429
1.6	49.0	−191	210.5	513

Table 5 summarizes the improvement obtained in wear behaviour and hardness property of processed BRC and IRC composites over the base alloy.

3.3.2 Influence of applied load

Wear graphs of LM13 alloy, BRC and IRC composites showed higher wear rates at higher applied loads for a given composition-sliding distance condition (as shown in Fig. 5 and given in Table 5). Under initial conditions of sliding, plastic deformation and fracturing of material occur and microcracks are developed beneath the contact surface. As sliding distance increases, propagation and convergence of these microcracks lead to the removal of material [5,7]. At higher loads, this mechanism dominates and delays the work hardening of material, and thus, causes higher wear rates. Further, in the case of steady state wear, increase in applied load affects the oxidation of worn surfaces and MML [2,37]. Higher applied load results in higher temperature at worn surfaces and higher oxidation rates of material. This results in the formation of a protective layer of oxides on the worn surface, preventing further wear [37]. However, higher loads also affect the stability of MML. At higher loads, the generation of microcracks is higher, causing the removal of material from MML [38]. The overall effect is the increase in wear rate at higher applied loads.

Table 5 Improvement in properties of AMCs over base alloy

Property of AMCs	Applied load/N	Change compared to base alloy/%					
		IRC composites			BRC composites		
		IRC-5	IRC-10	IRC-15	BRC-5	BRC-10	BRC-15
Reduction in maximum wear rate*	9.8	30	43	53	47	54	60
	29.4	31	40	51	44	55	61
	49.0	23	32	45	40	52	58
Increase in hardness (HRB)	−	31	45	50	34	50	56

*Tested at sliding distance of 500 m

3.3.3 Influence of reinforced particles

AMCs (both BRC and IRC) showed lower wear rate than the base alloy for any applied load-sliding distance condition. Further, drop in wear rate of AMCs was observed with the increase in content of reinforced particles. During sliding, dislocations are generated on the worn surface and their movement is blocked by secondary particles. This restriction by the reinforced ceramic particles or intermetallic compounds results in piling up of dislocations around the particles. The entrapment of dislocations around the secondary particles leads to the increase in strain hardening and resistance to plastic deformation, thus lowering the wear rate [6].

For a given reinforcement level and applied load-sliding distance condition, BRC composites showed superior wear characteristics than IRC composites (Table 5). B_4C particles have higher hardness (9.3, Mohs) in comparison to $FeTiO_3$ particles (5.0−6.0, Mohs) [14,39]. At a particular reinforcement level, the low density of B_4C (2.52 g/cm^3) leads to higher number of particles as compared to $FeTiO_3$ (4.72 g/cm^3). Hence, in the case of BRC composites, the entrapment of dislocation is higher, which corresponds to high strain hardening [6]. Also, MML is more stable in BRC composites because of their relatively higher hardness.

In the case of IRC composites, the maximum temperature (predicted using Eq. (3)) is attained much early as compared to BRC composites. This is attributed to the lower thermal conductivity of $FeTiO_3$ (1.49 W/(m·K)) in comparison to B_4C (30 W/(m·K)) [11,35]. Thus, the heat generated due to friction is dissipated to a lesser extent in IRCs causing relatively higher temperature at the pin surface. This results in early formation of oxide layer, and thus, prevents the wear of IRC composites. Also, as stated earlier, interfacial bonding formed by ilmenite particles was relatively stronger than the B_4C particles.

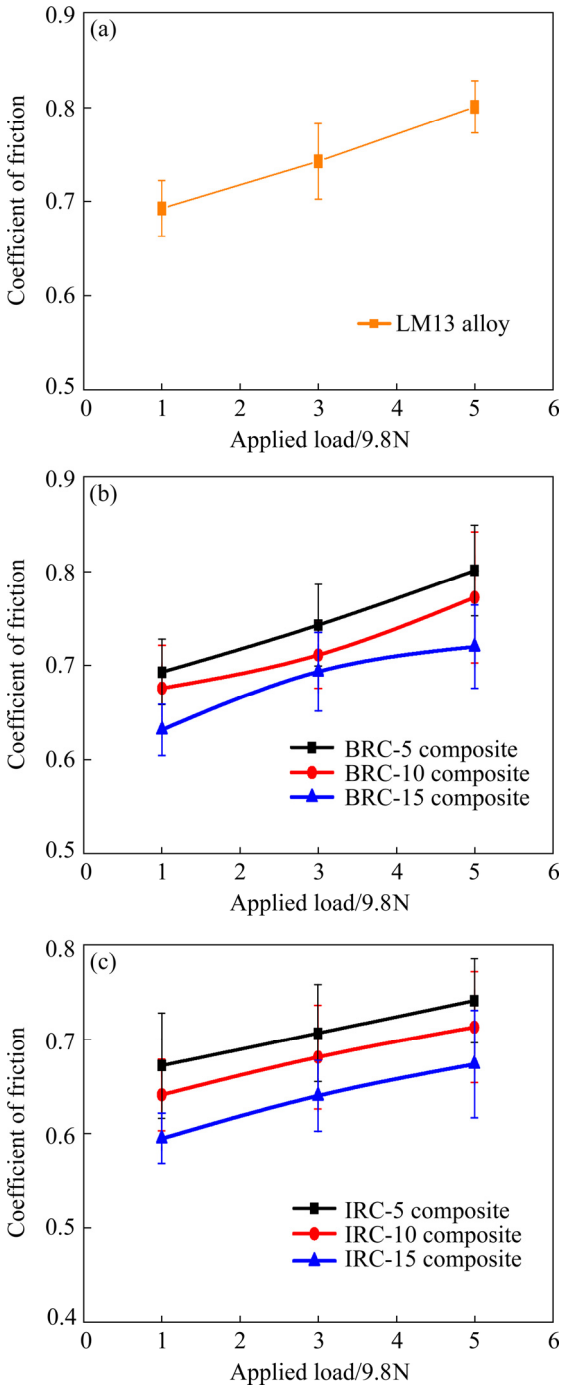

Fig. 6 Coefficient of friction for LM13 base alloy (a), BRC composites (b) and IRC composites (c)

3.4 Coefficient of friction

Figure 6 presents the coefficient of friction (COF) values for LM13 base alloy and processed composites under different applied load conditions. With the increase in mass fraction of reinforced particles (i.e. B_4C/ilmenite particles), a decreasing trend in COF values was observed. With the increase in applied load at a given reinforcement level, an increase in COF values was observed. At a given reinforcement level and applied load condition, IRC composites showed relatively lower COF values. The decrease in COF values with the addition of reinforced particles was attributed to (1) the reduction in area of contact of the matrix phase, and (2) the decrease in energy required for sliding of the surface due to reduced contact [40].

The increase in COF values with the increase in applied load was attributed to the increase in plastic deformation of sliding surfaces which exposed the composite pin surface to the steel disc (of tribometer). Lower COF values shown by IRC composites signified the lubricity effect of ilmenite particles [13,40]. This lubricity effect was attributed to early oxidation of sliding surface due to the lower thermal conductivity of ilmenite particles as discussed in Section 3.3.3 [40].

3.5 Analysis of wear-tracks and wear-debris

SEM micrographs of wear-tracks and wear-debris for BRC-15 and IRC-15 composites tested under the load of 49.0 N are shown in Fig. 7. Worn-out surfaces of AMCs showed the presence of delaminated area and grooves. There was relatively greater surface damage observed for IRC-15 composite (Figs. 7(a, b)). The greater surface damage in IRC composites was attributed to the presence of relatively larger number of micro-cracks and less stability of MML.

The presence of grooves on the worn surfaces signifies the entrapment of wear debris. The entrapment of wear particles results in three-body abrasive wear which ploughs the worn surface by hardened wear debris.

SEM images of wear debris of BRC-15 and IRC-15 composites revealed the formation of fractured debris, flake-like debris, micro-cuts, and oxides on debris (Figs. 7(c, d)). The average size of wear debris for BRC-15 composite was larger than that for IRC-15 composite, indicating larger numbers of microcracks and hence lower wear resistance in IRC composites under a given condition. The formation of flake-like debris justified the removal of material by microcracks as explained earlier. Micro-cuts/thread-like debris were obtained due to the abrasive action caused by trapped particles. Fractured-debris were obtained due to rupturing of trapped particles under applied load. The presence of oxides on debris signified the rise in temperature, which oxidised the sliding surface.

EDS analysis results of wear-tracks/wear-debris of AMCs are presented in Table 6.

IRC-15 composite showed the presence of aluminium, silicon, oxygen, iron, carbon, copper, and titanium on wear-tracks as well as wear-debris. BRC-15 composite showed the presence of aluminium, silicon, oxygen, iron, carbon, and copper. Interestingly, boron was not observed in BRC composites, maybe due to the low atomic number of boron which makes it difficult to detect in EDS analysis. The net amount of oxygen present on wear-track of IRC-15 composite (after deducting

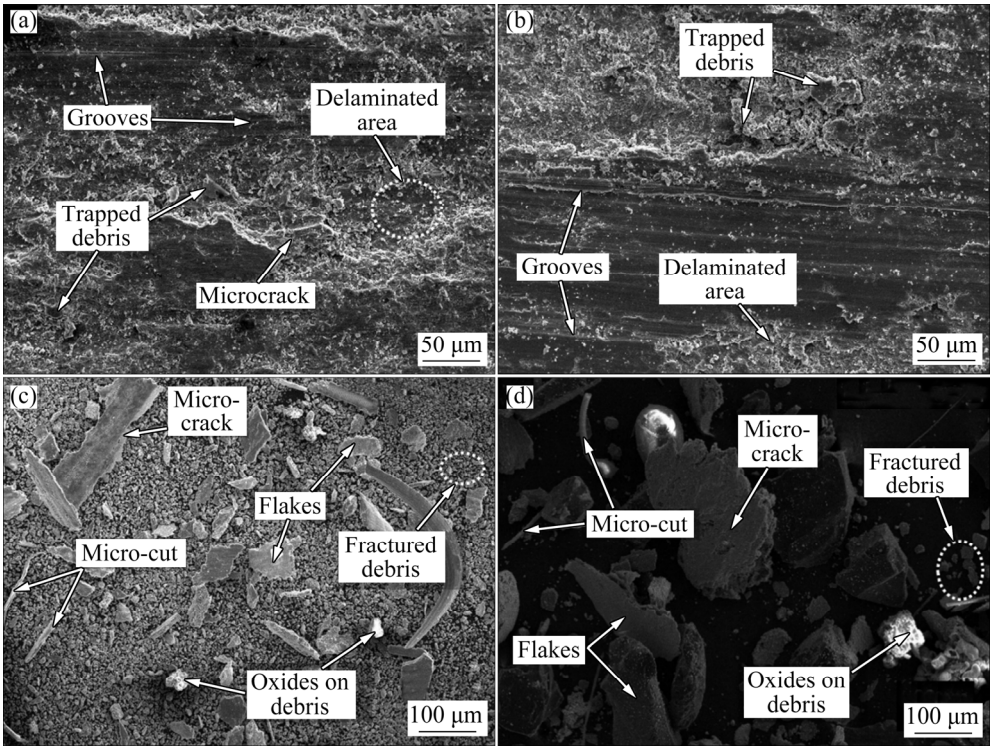

Fig. 7 SEM images of worn surface (a, b) and wear-debris (c, d) for IRC-15 (a, c) and BRC-15 (b, d) at 49.0 N load

Table 6 Contents of elements present on wear-track and wear-debris of AMCs

Zone	Composite	Content of element/wt.%						
		Al	Si	O	Fe	C	Cu	Ti
Wear-track	BRC-15	37.22	4.43	29.45	23.12	3.53	2.23	−
	IRC-15	44.09	5.50	26.02	18.02	2.70	2.03	1.64
Wear-debris	BRC-15	29.99	2.92	24.14	36.80	3.83	2.32	−
	IRC-15	31.44	4.00	34.03	16.85	10.53	1.70	1.45

the amount of oxygen present in ilmenite) was 21.10 wt.% which was lower than the BRC-15 composite (i.e. 29.45 wt.%). This signified that MML (which is a mixture of oxide particles) formed on the surface of BRC composites was relatively more stable. On the other hand, the relatively high amount of oxygen on wear debris of IRC-15 composite (net percentage of oxygen present was 29.68 wt.% after deducting the amount present in ilmenite) in comparison to BRC-15 composite (i.e. 24.14 wt.%) justifies the high oxidation rate in IRC composites. Further, the significant amount of iron and carbon on wear-tracks revealed the transfer of material from the counter-disc also. This transfer of material was higher in BRC-15 composite, which also signifies the formation of more stable MML on the worn surface of BRC composites. The presence of higher concentration of aluminium and silicon in wear debris of IRC-15 composites also indicates the relatively less stability of MML in IRC composites.

4 Conclusions

(1) Addition of ilmenite particles to the LM13 alloy resulted in the occurrence of interfacial reaction on the reinforced particles. So, ilmenite reinforced composites resulted in improved properties due to the strong interfacial bonding between matrix and reinforcement. However, the addition of boron carbide particles resulted in higher crystallinity, lower average crystallite size, and greater grain refinement, which were responsible for high hardness value. Further, both types of reinforcements influenced the silicon morphology, changing it from flake-like (for the base alloy) to globular (for the AMCs).

(2) For a given reinforcement level and applied load-sliding distance condition, BRC composites provided superior wear characteristics to IRC composites. However, in the case of coefficient of friction, IRC composites showed better results when compared to BRC composites. The low density and high hardness of B_4C particles resulted in high dislocation density around the filler particles in BRCs. IRC composites also resulted in significant improvement in wear and friction characteristics over the LM13 alloy. The low thermal conductivity of ilmenite particles caused early formation of oxide layer, and thus, prevented the wear of IRC composites.

(3) Both types of reinforcements led to significant improvements in wear characteristics of processed AMCs though the mechanisms involved in the two types of composites was very different. This research shows that the low-cost natural minerals (here, ilmenite) can act as an effective substitute to the high-cost synthetic ceramic fillers for processing of wear resistant AMCs.

Acknowledgments

The corresponding author is grateful to the Council of Scientific and Industrial Research (CSIR), New Delhi, India (Letter No. 22(0769)/18/ EMR-II) for the financial support of the present work.

References

[1] HARICHANDRAN R, SELVAKUMAR N, VENKATACHALAM G. High temperature wear behaviour of nano/micro B4C reinforced aluminium matrix composites fabricated by an ultrasonic cavitation-assisted solidification process [J]. Transactions of the Indian Institute of Metals, 2017, 70: 17−29.

[2] GUPTA R, SHARMA S, NANDA T, PANDEY O P. Wear studies of hybrid AMCs reinforced with naturally occurring sillimanite and rutile ceramic particles for brake-rotor applications [J]. Ceramics International, 2020, 46: 16849−16859.

[3] SAGHAFIAN H, SHABESTARI S G, GHADAMI S, GHONCHEH M H. Effects of iron, manganese, and cooling rate on microstructure and dry sliding wear behavior of LM13 aluminum alloy [J]. Tribology Transactions, 2017, 60:

888−901.

[4] POZDNIAKOV A V, LOTFY A, QADIR A, SHALABY E, KHOMUTOV M G, CHURYUMOV A Y, ZOLOTOREVSKIY V S. Development of Al−5Cu/B_4C composites with low coefficient of thermal expansion for automotive application [J]. Materials Science and Engineering A, 2017, 688: 1−8.

[5] LAKSHMIKANTHAN A, BONTHA S, KRISHNA M, KOPPAD P G, RAMPRABHU T. Microstructure, mechanical and wear properties of the A357 composites reinforced with dual sized SiC particles [J]. Journal of Alloys and Compounds, 2019, 786: 570−580.

[6] HABIBNEJAD-KORAYEM M, MAHMUDI R, GHASEMI H M, POOLE W J. Tribological behavior of pure Mg and AZ31 magnesium alloy strengthened by Al_2O_3 nano-particles [J]. Wear, 2010, 268: 405−412.

[7] XIAO P, GAO Y, XU F, YANG C, LI Y, LIU Z, ZHENG Q. Tribological behavior of in-situ nanosized TiB_2 particles reinforced AZ91 matrix composite [J]. Tribiology International, 2018, 128: 130−139.

[8] TIWARI S, DAS S, CH V A N. Mechanical properties of Al−Si−SiC composites [J]. Materials Research Express, 2019, 6: 076553.

[9] ZENG X, TENG J, YU J G, TAN A S, FU D F, ZHANG H. Fabrication of homogeneously dispersed graphene/Al composites by solution mixing and powder metallurgy [J]. International Journal of Minerals, Metallurgy and Materials, 2018, 25: 102−109.

[10] SAESSI M, ALIZADEH A, ABDOLLAHI A. Wear behavior and dry sliding tribological properties of ultra-fine grained Al5083 alloy and boron carbide-reinforced Al5083-based composite at room and elevated temperatures [J]. Transactions of Nonferrous Metals Society of China, 2021, 31: 74−91.

[11] GRASSO S, HU C, VASYLKIV O, SUZUKI T S, GUO S, NISHIMURA T, SAKKA Y. High-hardness B4C textured by a strong magnetic field technique [J]. Scripta Materialia, 2011, 64: 256−259.

[12] PRABHU S R, SHETTIGAR A K, HERBERT M A, RAO S S. Microstructure and mechanical properties of rutile-reinforced AA6061 matrix composites produced via stir casting process [J]. Transactions of Nonferrous Metals Society of China, 2019, 29: 2229−2236.

[13] GUPTA R, SHARMA S, NANDA T, PANDEY O P. A comparative study of dry sliding wear behaviour of sillimanite and rutile reinforced LM27 aluminium alloy composites [J]. Materials Research Express, 2019, 7: 016540.

[14] EBRAHIMIAN-HOSSEINABADI M, AZARI-DORCHEH K, VAGHEFI S M M. Wear behavior of electroless Ni−P−B_4C composite coatings [J]. Wear, 2006, 260: 123−127.

[15] AO M, LIU H, DONG C. The effect of La_2O_3 addition on intermetallic-free aluminium matrix composites reinforced with TiC and Al_2O_3 ceramic particles [J]. Ceramics International, 2019, 45: 12001−12009.

[16] LIU Y X, WANG R C, PENG C Q, CAI Z Y, ZHOU Z H, LI X G, CAO X Y. Microstructures and mechanical properties of in-situ TiB_2/Al−xSi−0.3Mg composites [J]. Transactions of Nonferrous Metals Society of China, 2021, 31: 331−344.

[17] MONIKANDAN V V, RAJENDRAKUMAR P K, JOSEPH M A. High temperature tribological behaviors of aluminum matrix composites reinforced with solid lubricant particles [J]. Transactions of Nonferrous Metals Society of China, 2020, 30: 1195−1210.

[18] SINGH R K, TELANG A, DAS S. Microstructure, mechanical properties and two-body abrasive wear behaviour of hypereutectic Al−Si−SiC composite [J]. Transactions of Nonferrous Metals Society of China, 2020, 30: 65−75.

[19] SHAYAN M, EGHBALI B, NIROUMAND B. Fabrication of AA2024−TiO_2 nanocomposites through stir casting process [J]. Transactions of Nonferrous Metals Society of China, 2020, 30: 2891−2903.

[20] NIE C Z, GU J J, LIU J L, ZHANG D. Investigation on microstructures and interface character of B_4C particles reinforced 2024Al matrix composites fabricated by mechanical alloying [J]. Journal of Alloys and Compounds, 2008, 454: 118−122.

[21] BARADESWARAN A, PERUMAL A E. Influence of B_4C on the tribological and mechanical properties of Al 7075-B_4C composites [J]. Composites Part B: Engineering, 2013, 54: 146−152.

[22] TORRES B, LIEBLICH M, IBÁÑEZ J, GARCÍA-ESCORIAL A. Mechanical properties of some PM aluminide and silicide reinforced 2124 aluminium matrix composites [J]. Scripta Materialia, 2002, 47: 45−49.

[23] SHARMA S, NANDA T, PANDEY O P. Effect of dual particle size (DPS) on dry sliding wear behaviour of LM30/ sillimanite composites [J]. Tribology International, 2018, 123: 142−154.

[24] ZENG X, YU J G, FU D F, ZHANG H, TENG J. Wear characteristics of hybrid aluminum-matrix composites reinforced with well-dispersed reduced graphene oxide nanosheets and silicon carbide particulates [J]. Vacuum, 2018, 155: 364−375.

[25] RAGHAVENDER A T, HONG N H, LEE K J, JUNG M H, SKOKO Z, VASILEVSKIY M, CERQUEIRA M F, SAMANTILLEKE A P. Nano-ilmenite $FeTiO_3$: Synthesis and characterization [J]. Journal of Magnetism and Magnetic Materials, 2013, 331: 129−132.

[26] CHEN G, SONG Z K, CHEN J, PENG J H, SRINIVASAKANNAN C. Evaluation of the reducing product of carbonthermal reduction of ilmenite ores [J]. Journal of Alloys and Compounds, 2013, 577: 610−614.

[27] MALEKI A, NIROUMAND B, SHAFYEI A. Effects of squeeze casting parameters on density, macrostructure and hardness of LM13 alloy [J]. Materials Science and Engineering A, 2006, 428: 135−140.

[28] HOSSEINI V A, SHABESTARI S G, GHOLIZADEH R. Study on the effect of cooling rate on the solidification parameters, microstructure, and mechanical properties of LM13 alloy using cooling curve thermal analysis technique [J]. Materials and Design, 2013, 50: 7−14.

[29] MALEKI A, SHAFYEI A, NIROUMAND B. Effects of squeeze casting parameters on the microstructure of LM13 alloy [J]. Journal of Materials Processing Technology, 2009, 209: 3790−3797.

[30] SEONG H G, LOPEZ H F, ROBERTSON D P, ROHATGI P K. Interface structure in carbon and graphite fiber reinforced 2014 aluminum alloy processed with active fiber cooling [J]. Materials Science and Engineering A, 2008, 487: 201−209.
[31] THAM L M, GUPTA M, CHENG L. Effect of limited matrix-reinforcement interfacial reaction on enhancing the mechanical properties of aluminium−silicon carbide composites [J]. Acta Materialia, 2001, 49: 3243−3253.
[32] SONG F Z, WANG Q H, WANG T M. The effects of crystallinity on the mechanical properties and the limiting *PV* (pressure × velocity) value of PTFE [J]. Tribiology International, 2016, 93: 1−10.
[33] ABBAS A, HUANG S J. Qualitative and quantitative investigation of as-cast and aged CNT/AZ31 metal matrix composites [J]. JOM, 2020, 72: 2272−2282.
[34] ABBAS A, HUANG S J. Investigation of severe plastic deformation effects on microstructure and mechanical properties of WS2/AZ91 magnesium metal matrix composites [J]. Materials Science and Engineering A, 2020, 780: 139211.
[35] CLAUSER C, HUENGES E. Thermal conductivity of rocks and minerals [J]. Rock Physics and Phase Relations: A Handbook of Physical Constants, 1995, 3: 105−126.
[36] LINTON J, NAVROTSKY A, FEI Y. The thermodynamics of ordered perovskites on the $CaTiO_3$−$FeTiO_3$ join [J]. Physics and Chemistry of Minerals, 1998, 25: 591−596.
[37] CHEN H, ALPAS A T. Sliding wear map for the magnesium alloy Mg−9Al−0.9Zn (AZ91) [J]. Wear, 2000, 246: 106−116.
[38] ZHOU H B, YAO P P, XIAO Y L, FAN K Y, ZHANG Z Y, GONG T M, ZHAO L, DENG M W, LIU C, LING P. Friction and wear maps of copper metal matrix composites with different iron volume content [J]. Tribiology International, 2019, 132: 199−210.
[39] ABDOU M I, AL-SABAGH A M, AHMED H E, FADL A M. Impact of barite and ilmenite mixture on enhancing the drilling mud weight [J]. Egyptian Journal of Petroleum, 2018, 27: 955−967.
[40] ZHU H G, JAR C C, SONG J Z, ZHAO J, LI J L, XIE Z H. High temperature dry sliding friction and wear behavior of aluminum matrix composites (Al_3Zr+α-Al_2O_3)/Al [J]. Tribology International, 2012, 48: 78−86.

合成 B_4C 和天然钛铁矿陶瓷颗粒增强 LM13 铝硅合金基复合材料的磨损性能对比

Rahul GUPTA[1], Tarun NANDA[1], O. P. PANDEY[2]

1. Mechanical Engineering Department, Thapar Institute of Engineering and Technology, Patiala 147004, Punjab, India;
2. School of Physics and Materials Science, Thapar Institute of Engineering and Technology, Patiala 147004, Punjab, India

摘　要：研究以 LM13 铝硅合金为基体、陶瓷颗粒为增强相，采用搅拌铸造法制备的复合材料(AMCs)的干滑动磨损行为。分别采用两种不同的陶瓷颗粒增强相：合成的 B_4C 和天然的钛铁矿陶瓷颗粒。光学显微镜结果显示，增强颗粒均匀分散在基体材料中，增强颗粒使共晶硅的晶粒尺寸细化，形貌变为球形。B_4C 增强复合材料(BRCs)的硬度提高最大，而钛铁矿增强复合材料(IRCs)由于界面化合物的形成导致基体−增强相界面结合较强，摩擦因数降低最大。与基体合金相比，复合材料的干滑动磨损性能显著提高。B_4C 颗粒的低密度和高硬度导致 BRCs 中颗粒周围高的位错密度。另一方面，钛铁矿颗粒的低热导率导致 IRCs 表面发生早期氧化并形成摩擦层。可见，尽管两种类型的增强相的作用机制存在很大不同，他们都能改善 AMCs 的耐磨性能。因此，低成本钛铁矿颗粒可替代高成本 B_4C 颗粒，制备耐磨复合材料。

关键词：铝基复合材料；钛铁矿；碳化硼；颗粒增强体；磨损测试；摩擦层；XRD 分析；SEM−EDS

(Edited by Bing YANG)